A low-temperature ultrahigh vacuum scanning force microscope with a split-coil magnet

M. Liebmann, A. Schwarz, S. M. Langkat, and R. Wiesendanger
Institute of Applied Physics and Microstructure Research Center, University of Hamburg, Jungiusstrasse 11, D-20355 Hamburg, Germany

(Received 8 March 2002; accepted for publication 24 June 2002)

We present the design of a scanning force microscope, which is optimized for magnetic force microscopy experiments. It can be operated at temperatures down to 5.2 K, in ultrahigh vacuum, and in magnetic fields of up to 5 T. Cooling is provided by a liquid helium bath cryostat, and the magnetic field is generated by a superconducting split-coil magnet. The design allows easy access from the side through a shutter system for fast *in situ* tip and sample exchange, while the microscope stays at temperatures below 25 K. The microscope itself features an all-fiber interferometric detection system, a $7.5\times7.5\ \mu m^2$ scan area at 5.2 K, and an *xy* table. The topographic resolution is demonstrated by imaging monoatomic steps on a nickel oxide surface, while magnetic contrast is shown on cobalt platinum multilayers and on a manganite perovskite film. © *2002 American Institute of Physics.* [DOI: 10.1063/1.1502446]

I. INTRODUCTION

Since the first successful operation of a scanning force microscope (SFM),[1] this technique has been applied in different environments. From the viewpoint of surface science and investigation of basic processes in solid state physics, it is promising to extend this powerful tool of real space imaging to low temperatures in conjunction with high magnetic fields, and to combine it with preparation and analysis techniques in an ultrahigh vacuum (UHV) environment. In particular, such an instrument allows to study the large variety of magnetic phenomena by using magnetic force microscopy (MFM).

Several successful attempts have been made to operate a SFM at temperatures as low as liquid nitrogen or helium. One possibility is the cooling of the sample by connecting it to a heat sink via a cold finger. Operation has been reported in high vacuum[2,3] and in ultra high vacuum.[4,5] Such a setup provides relatively easy access to the microscope for tip and sample exchange and for adjusting the signal detection mechanism.

A major disadvantage of the cold finger method is the presence of large temperature gradients. To benefit from the reduced thermal noise of the cantilever and from the increased stability at low temperatures, one has to use a bath cryostat, which keeps the whole microscope in a cold environment.[6–20] With liquid helium as a refrigerant, a superconducting magnet can be implemented to apply large magnetic fields.[13,16–19] Some of these instruments have been used for MFM experiments.[8–10,16,18,19]

To install a SFM in an UHV environment at low temperatures, is a challenging task. The combination of bakability, low vapor pressure, and matching of thermal contraction coefficients strongly limits the choice of materials. So far, it has only been realized by very few groups.[7,12,16,20] With such bath cryostat designs, very low noise and stable imaging conditions have been achieved. *True* atomic resolution on indium arsenide,[21] graphite,[22] xenon,[23] nickel oxide,[24] and silicon[25,26] has been demonstrated.

Up to now, the only instrument, which combines ultrahigh vacuum, low temperatures, *in situ* preparation, and a superconducting magnet is described in Ref. 16. It features a bath cryostat beneath the sample transfer level. For tip or sample exchange, the whole microscope has to be disconnected from its thermal anchoring and lifted up.

In this article, we present a scanning force microscope, optimized for MFM measurements, with a large scan area, a modular design, and interferometric detection of the cantilever deflection. The instrument is placed in an UHV compatible top bath cryostat with a superconducting magnet. This setup keeps the microscope in the transfer level of the UHV system. Easy access is provided by using a split-coil magnet and two shutters in front of a cutaway through the liquid helium tank. Thereby, the microscope remains fixed to its thermal anchoring during *in situ* tip or sample exchange, which allows a fast, safe, and reliable operation.

II. UHV SYSTEM

To study clean surfaces with well defined tips, the opportunity of *in situ* preparation like cleavage, heating, sputtering, and evaporation is essential. Therefore, the scanning force microscope is part of an UHV system consisting of three chambers.

The cryostat chamber with the superconducting magnet and the microscope are described in more detail in the following sections. Tip and sample treatment is accomplished in the preparation chamber,[27] which is equipped with an electron beam heating, a sputter gun with a differential pumping line, an iron evaporation cell, and a resistive or direct current heating. The analysis chamber[27] contains a surface analysis unit for low energy electron diffraction and Auger electron spectroscopy.

To introduce cantilevers and samples into the UHV system, a load lock is connected to the preparation chamber. Access to the different chambers is provided by magnetic linear and rotary motion drives with perpendicular handing over. Sample holders in the preparation and analysis chamber can be positioned by *xyz* manipulators. In particular, the orientation of the tip towards the sputter gun and the iron evaporator can be adjusted precisely.

To achieve pressures better than 10^{-8} Pa, the UHV system is baked at 120 °C for three days, while the temperature of the superconducting magnet has to be kept below 100 °C. During bakeout, the vacuum system is pumped by three turbo pumps,[28] one for the cryostat, the preparation chamber, and the load lock each. Thereafter, ultrahigh vacuum is maintained by three ion getter[29] and three titanium sublimation pumps[30] (one for each chamber).

In order to realize a sufficient vibration isolation of the microscope from external noise sources, the UHV system is mounted on pneumatic damping legs which in turn stand on a separate foundation. During measurements, all mechanical pumps are switched off, and the experimentator stays in an adjacent room. Due to the rigid microscope design (see Sec. V), no additional internal damping stage for the microscope inside the cryostat is needed.

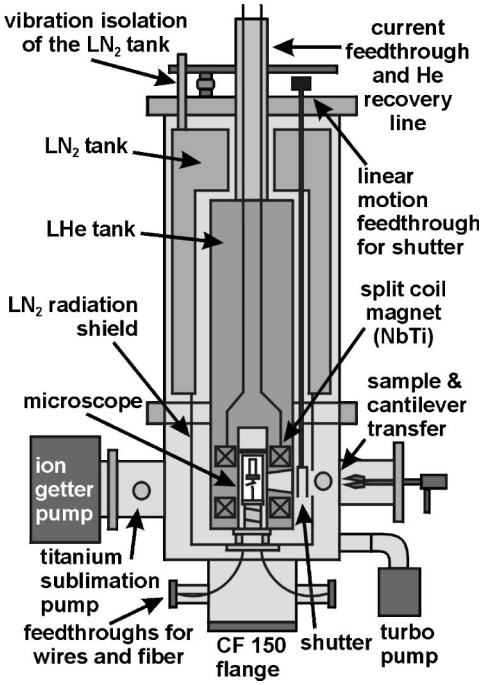

FIG. 1. Cross section of the magnet cryostat. The microscope is inserted from below together with the microscope chamber containing the electrical and fiber-optical feedthroughs.

III. MAGNET CRYOSTAT

The design of the magnet cryostat is guided by the demand for a strong magnetic field, combined with easy and fast access to the microscope and reliable operation. This is best attained, if the microscope is located in the transfer level of the UHV system. Therefore, we chose a liquid helium (LHe) top bath cryostat with a liquid nitrogen (LN_2) radiation shield and a superconducting split-coil magnet. The microscope right in the center of the magnet is described in Sec. V.

A cross section of the cryostat chamber is shown in Fig. 1. The magnet cryostat[31] fits into a DN 450 COF flange on top of the cryostat chamber.[30] A separate microscope chamber with all necessary feedthroughs for the operation of the microscope is connected via a DN 250 flange at the bottom. Viewports offer optical access to the microscope under various angles, when the shutters are opened, thus facilitating coarse approach and exchange of tip and sample with a wobble stick.

The cryostat consists of two tanks for cooling liquids. The outer tank serves as a radiation shield and is filled with up to 35.5 ℓ of liquid nitrogen. It is mechanically decoupled from the vacuum chamber by viton stacks and edge welded bellows. A pump line can be added for solidifying the nitrogen in order to minimize perturbations due to the boiling refrigerant. Below the LN_2 tank, a gold coated copper radiation shield is mounted, which encloses the lower part of the LHe tank.

The inner tank includes the magnet and is filled with up to 33.5 ℓ of LHe which yields a hold time of 48 h. The current feedthroughs for the magnet, which are capable of 100 A, run through the tank and the exhaust dome and are thus directly cooled by the evaporating cryogen. Additionally, they may be disconnected inside the tank and retracted during persistent operation of the magnet. Two 50 W resistive heaters with PT100 temperature sensors are mounted on the bottom of the LHe tank. They are used to evaporate any remaining cryogen after the magnet has been precooled with liquid nitrogen, and to assist the bakeout procedure. Moreover, it enables variable temperature measurements up to a certain degree by heating the large thermal mass of the magnet. Two additional PT100 temperature sensors are fixed to the side face of the magnet to measure the magnet temperature during bakeout and cooling.

The magnet[32] has a split-coil geometry with a central bore of 60 mm in diameter, which hosts the microscope. With its superconducting NbTi coils, it produces a maximum field of 5 T vertical, which is perpendicular to the sample surface. The homogeneity is specified to be better than 5×10^{-3} within a 10 mm diameter at the sample location. Field ramping at rates down to 0.6 mT/min is possible with the currently used control unit.

In order to exchange tip and sample without moving the microscope, there has to be an access from the side through the radiation shield and the LHe tank to the microscope in the center of the magnet. This is provided by an 80° cutaway with a height of at least 40 mm between the two magnet coils. The cutaway can be closed by two copper shutters, which are moved simultaneously by a linear motion feedthrough operated from the top of the cryostat. They are thermally connected with stranded copper wires to the LHe and LN_2 tank, respectively, and gold coated to reduce thermal radiation.

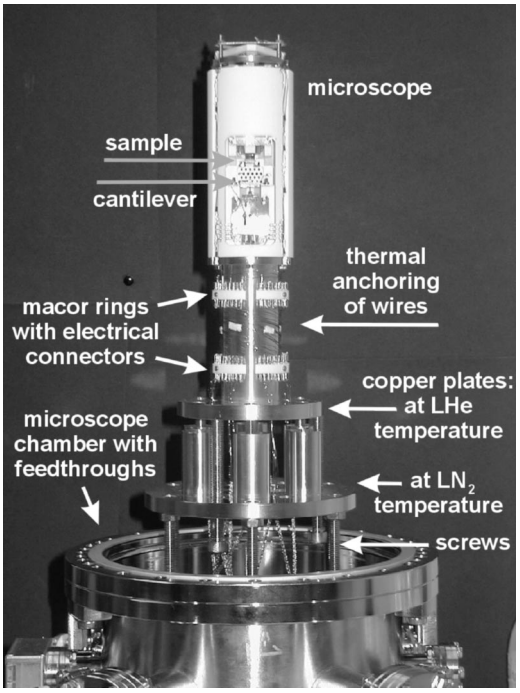

FIG. 2. Thermal anchoring of the microscope. During insertion, the copper parts are connected via screws to the microscope chamber, but disconnected afterwards (see the text).

IV. THERMAL ANCHORING, ELECTRICAL AND OPTICAL CONNECTIONS

To reach a low final temperature and a short cooling time, the thermal conductivity from the microscope to the cryogen has to be maximized, and the thermal load from room temperature has to be minimized. Heat transfer through the electrical connections and pressed contacts has to be considered as well as thermal radiation.[33]

Figure 2 shows a photo of the microscope and its thermal anchoring. In the lower part, the microscope chamber is visible, which contains the side flanges for all feedthroughs of the electrical connections and the fiber. The copper parts with the microscope body on top are connected to the LN_2 radiation shield and the LHe tank (see below). Up to now, no UHV compatible detachable fiber connections are available. Therefore, the whole setup has to be mounted from below into the bore of the cryostat. During insertion, the microscope chamber is held by a cardanic suspension, which allows to adjust the microscope position very carefully with respect to the central bore of the magnet. This procedure is needed, because the diameter of the microscope (58 mm) is only 2 mm less than that of the magnet bore. After insertion, the screws, which connect the copper parts to the microscope chamber, are removed through a CF 150 flange at the bottom (see Fig. 1).

The microscope is screwed to an oxygen-free high-conductivity copper cylinder with a cylindrical ground plate, which in turn is screwed to the bottom of the LHe tank. Another copper plate is screwed to the bottom of the LN_2 radiation shield. To enhance the reliability of the connections and to achieve higher contact pressures, heli coils are used in all copper threads of the LHe tank and the LN_2 radiation shield. To improve the thermal conductivity through the pressed contacts, the copper parts are gold coated.[34,35] Moreover, the gold coating prevents oxidation of the copper parts and reduces thermal radiation.

The copper cylinder serves as a thermal anchoring of the electrical wires[36] as well, which are glued to it over a length of 10 mm. Below and above these glue points, there are two rings of electrical connectors. Thus it is possible to detach the microscope from the copper base without destroying the thermal anchoring of the wires. Further anchoring is not useful due to the small distance between LN_2 and LHe temperature parts.

All electrical connections between room temperature and LHe temperature are made out of manganin wires (0.1 mm diameter) because of their reduced thermal conductivity compared to copper. Corresponding wires such as tip-sample bias are twisted. For electrical shielding and protection, they are guided through the two cylindrical copper plates in copper beryllium meshes towards the feedthrough flanges at the microscope chamber. The optical fiber for the detection of cantilever displacement is directed through the center of the microscope and the copper base. It ends outside the chamber after passing a small bore in which it is glued with UHV compatible epoxy resin.[37]

With LHe cooling and closed shutters, a temperature of 5.2 K is routinely achieved. Main heat sources are the nearly 50 wires needed to operate the microscope, and thermal radiation from the shutters, which do not have exactly the same temperature as the refrigerant. With opened shutters during tip or sample exchange, the temperature usually stays below 25 K and returns to thermal equilibrium within 1 h. Initial cooling from room temperature to 78 K takes 12 h, and 4 h from 78 K down to 5.2 K, due to the large thermal mass of the magnet.

V. MICROSCOPE DESIGN

The operation of a microscope in UHV, at low temperatures, and in strong magnetic fields requires careful consideration of the possible materials. For UHV compatibility, a low vapor pressure and bakability up to 150 °C are necessary. For low temperature applications, one has to regard the matching of thermal contraction coefficients of different materials to avoid mechanical stress during cool down. In particular, strong magnetic fields and MFM experiments require nonmagnetic components. These properties are almost perfectly fulfilled by the used combination of the piezoelectric material lead zirconate titanate (PZT), macor,[38] and titanium.[39]

A schematic cross section of the microscope is given in Fig. 3. To keep the microscope as rigid as possible, the main body is made out of one piece of macor. It has a cylindrical shape of 125 mm in length and 58 mm in diameter. The fixed cantilever stage is located in the middle of the macor body. The upper part hosts the approach mechanism for the sample.

The lower part of the microscope contains the mechanism for the detection of cantilever deflections. We chose a fiber optic interferometer based on the setup given in Refs. 12 and 40, because it allows a very compact and rigid design

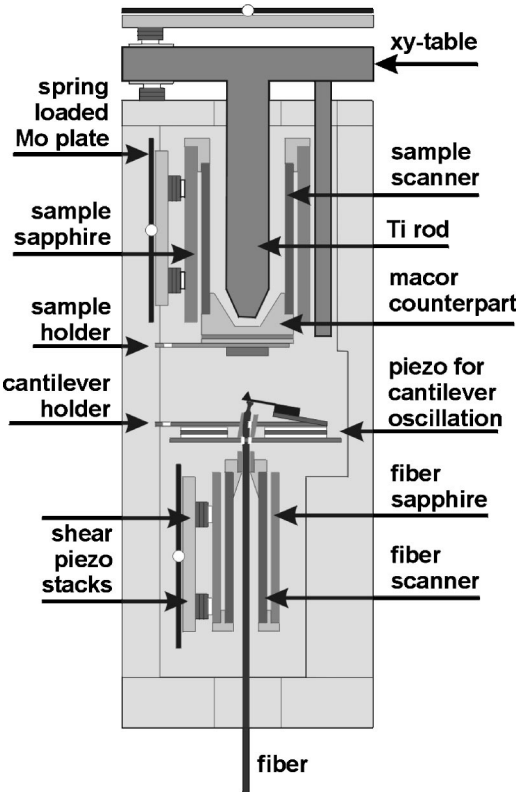

FIG. 3. Cross section of the microscope. A detailed description of all components can be found in the main text.

and is, at the same time, a very sensitive method. Light emitted by a laser diode[41] is guided through an optical single mode fiber and is backreflected into the fiber by the backside of the cantilever. This allows to keep the laser diode, the photodetector, and the amplification circuit at room temperature and outside of the vacuum chamber. Since the deflection signal is transported by light to the photodetector, it is not affected by any electromagnetic noise sources like stray fields from the electrical signals used to operate the microscope. As the wavelength of the laser light is known, one has a direct calibration of the cantilever deflection, which is necessary for quantitative measurements.

The well matched thermal expansion coefficient of the used microscope materials (see above) and the symmetry of the microscope along the cantilever axis avoid a lateral misalignment between fiber and cantilever during the cool down process. Therefore, only the separation between cantilever and fiber has to be readjusted. Coarse positioning is provided by a walker step motor as described below. Fine adjustment to the most sensitive point of the interferometer is realized by means of a piezoelectric scanner that holds the very end of the fiber and allows a vertical displacement of ± 400 nm at low temperatures. The fiber scanner also allows ± 10 μm lateral adjustment, but due to our reliable *ex situ* cantilever positioning and the symmetric microscope design, this facility is usually not needed.

Cantilevers are glued on commercially available cantilever holders[42] and are inserted into a fixed pick-up stage. This stage is mounted on top of a wobble piezo providing the oscillation of the cantilever in the dynamic force microscopy mode.

The above mentioned *ex situ* cantilever positioning mechanism is realized as follows: Before inserting the microscope into the cryostat, a cantilever is directly glued onto and aligned on a cantilever holder, which is already inserted into the pick-up stage in the microscope. This well aligned cantilever is used as a master in a second identical stage. From this master cantilever, an alignment mask is made, and other cantilevers can be glued *ex situ* by means of an optical microscope.

Samples are mounted on a small titanium plate, which can be inserted into the sample holder using a wobble stick. It is held on the sample scanner by two springs. A grounded layer of conducting glue prevents crosstalk between the scan voltage and the tip-sample bias. The sample scanner as well as the fiber scanner has gold electrodes and is made of EBL 4 piezoelectric material.[43] This type is reported to have small hysteresis and creep effects.[44] The dimensions of the sample scanner are 6.35 mm in diameter and 58 mm in length. Its lowest resonance frequency is about 700 Hz, which approximately matches the predicted value calculated from Ref. 45.

Coarse approach of sample and fiber towards the cantilever is realized by two single axis piezoelectric step motors based on the walker principle.[46,47] Fiber and sample scanner are glued into the bore of a sapphire prism each, which is held by six stacks of piezo plates. This configuration has already been described in Ref. 12 for a very similar microscope design. For sample exchange, the sample walker is fully retracted. At the end position, the conical end of a titanium rod fits precisely into a counterpart at the backside of the sample holder, thus absorbing the force applied to the scanner during sample exchange.

For lateral coarse positioning of the sample relative to the tip, an *xy* table is implemented in the microscope (Fig. 4). The walker housing with the sample coarse approach mechanism is mounted on a titanium disk, which can be moved by six piezo stacks. Three stacks are glued on a triangular macor plate, while the other three are glued on the top of the main microscope body. Each piezo stack consists of four shear piezos: two for the *x* and two for the *y* direction. For the two axis lateral movement of the titanium disk, the walker principle is used, analogous to the single axis movement described above. The load on the disk, and thereby the step width of the walker, can be adjusted by a molybdenum leaf spring, which presses onto the triangular macor plate via a ruby ball and is held by three screws on thread rods sticking out of the main body. Due to the high maximum pressures allowed by this design without preventing an *xy* motion, the microscope keeps its overall stability. The *xy* table can be moved within a 4×4 mm^2 area.

Lateral calibration of the scanner was accomplished by means of a silicon test grid[48] and yields scan ranges of 18×25 μm^2 at room temperature (RT), 15.5×18 μm^2 at 78 K, and 7.5×7.5 μm^2 at 5.2 K with a voltage of ± 130 V applied to the piezo electrodes. Additionally, a compact disk, the fiber optic interferometer, and monoatomic steps on a NiO surface (see Sec. VI) are used for *z* calibration.

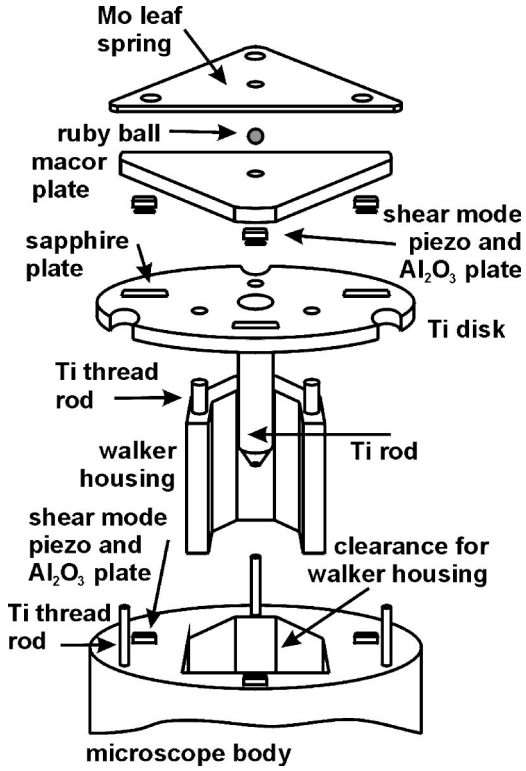

FIG. 4. Exploded view of the *xy* table. The walker housing is screwed to the titanium disk. The molybdenum leaf spring is held by screw nuts on the thread rods and determines the load on the titanium disk via the macor plate and the ruby ball. The *xy* table with the walker housing can easily be removed in order to change the scanner.

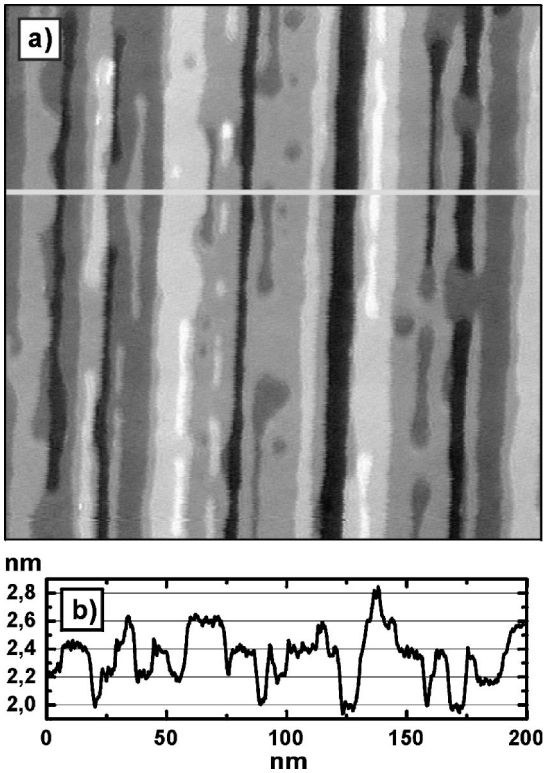

FIG. 5. (a) Topographic image of the (001) surface of an *in situ* cleaved and annealed NiO single crystal. Data acquisition has been performed after solidifying the LN_2 to avoid noise due to bubbling. Monoatomic steps (208 pm) are clearly resolved. (b) Display of a single scan line of image (a). Parameters: Scan area 200×200 nm^2, $T=5.2$ K, $f_0=192$ kHz, $\Delta f=-10$ Hz, $A=\pm5$ nm, $U_{\text{bias}}=1.1$ V, scan speed 222 nm/s, and bandwidth 300 Hz.

In the microscope, only copper wires (0.127 mm diameter) are used. All metallic parts are grounded. Permanent electrical connections are glued with silver epoxy or soldered. Removable connections use gold coated integrated circuit (IC) pins.

The temperature is monitored by a Cernox temperature sensor[49] attached to the microscope body next to the sample position. Magnetic fields of up to 5 T change the temperature reading of this sensor type by less than 0.2%.

VI. FIRST EXPERIMENTAL RESULTS

Both atomic and magnetic force microscopy mode benefit from the enhanced sensitivity of cantilever frequency detection due to their much higher quality factor in vacuum. All images presented in this section show raw data and are recorded with the frequency modulation technique described in Ref. 50. The thermal limit of the detectable frequency shift δf is given by

$$\langle(\delta f)^2\rangle=\frac{f_0 k_B T B}{\pi k_L Q A^2}, \tag{6.1}$$

where f_0 denotes the resonance frequency of the free cantilever, k_L the spring constant, Q the quality factor, k_B the Boltzmann constant, T the temperature, B the measurement bandwidth, and A the oscillation amplitude.[50]

At room temperature, we typically achieve a frequency resolution of 40 mHz_{rms} (oscillation amplitude $A=\pm5$ nm, bandwidth $B=100$ Hz) matching the thermodynamical limit calculated from Eq. (6.1). At 5.2 K, the rms noise δf amounts to 30 mHz_{rms}, which exceeds the thermodynamical limit by a factor of 5–8. In both cases, δf is proportional to $1/A$. The main contribution to the noise at low temperatures is given by the preamplifier electronics (e.g., shot noise in the photodiode) and scales with the square root of optical power hitting the photodiode. Therefore, an increase of the oscillation amplitude, laser power, or backreflection from fiber and cantilever would improve the signal-to-noise ratio.

For imaging, commercially available silicon cantilevers with resonance frequencies of 183–203 kHz and force constants of 40–57 N/m are used. To remove the native oxide layer, they have been sputtered with argon ions. During measurements, the amplitude A of the self-oscillating cantilever is kept constant by means of an amplitude regulator.

The z resolution of the instrument is demonstrated by imaging the (001) surface of an *in situ* cleaved NiO single crystal subsequently heated to 500 °C. The image displayed in Fig. 5 has been acquired at 5.2 K while pumping on the LN_2 tank, which effectively removes stochastic noise due to bubbling nitrogen. The measured step heights correspond to the half of the lattice constant (417 pm). Within each terrace, we observed a z noise of 22 pm_{rms}.

Magnetic imaging is usually performed by iron coating on that side of the tip pyramid, which faces the cantilever substrate. This results in a thin iron film of prolonged triangular shape with a magnetization along its symmetry axis. We found that such tips are nearly exclusively sensitive to

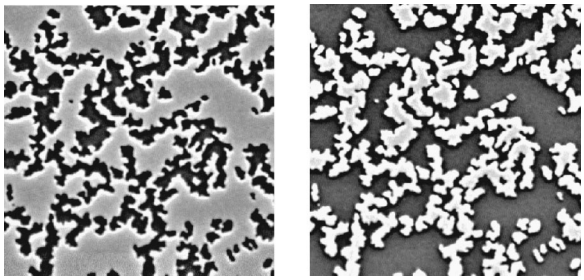

FIG. 6. MFM image of a CoPt multilayer sample. Both images are acquired at zero field and at the same location. The image on the right is recorded after applying 50 mT in order to reverse the tip magnetization. The domain structure remains unchanged, but the contrast is inverted. Parameters: scan area 7×7 μm^2, $T=5.2$ K, $f_0=201$ kHz, $A=\pm5$ nm, $h=30$ nm, $U_{bias}=20$ mV, gray scale 400 mHz, scan speed 5 μm/s, bandwidth 100 Hz, and $\delta f_{noise}=42$ mHz_{rms}.

the out-of-plane component of the sample stray field and exhibit a vanishing small in-plane component. The appropriate thickness of the iron film depends on the magnetic characteristics of the sample and should be a compromise between signal strength and minimized disturbance of the sample magnetization.

For MFM measurements, we apply the plane-subtraction mode: In the topographic mode (feedback on), the sample slope is compensated by adding appropriate voltages to the *z* electrode of the sample scanner. Thereafter, the feedback is switched off, and the tip is retracted from the sample surface to a scanning height *h* of typically 20–30 nm. A MFM image is obtained by scanning in this plane and recording the frequency shift, which is in this case dominated by long range forces of electrostatic or magnetostatic nature. The electrostatic contribution can be minimized by applying a bias voltage to compensate for the contact potential difference.

To characterize our MFM tips and demonstrate the out-of-plane sensitivity, we imaged a CoPt multilayer sample (Fig. 6) which has a strong perpendicular anisotropy. Both images are taken at the same tip-sample separation, with a bias voltage of 20 mV, and at zero magnetic field. The tip was coated with 5 nm iron on the side face towards the cantilever and 2.4 nm on the two outer sides of the tip pyramid. The CoPt sample has a much higher coercive field than the iron film on the tip. So it was possible to reverse the magnetization of the tip by applying a vertical magnetic field of 50 mT without changing the domain structure of the sample. This causes an inversion of contrast in the MFM image. The dark and bright edges next to the domain walls originate from a small in-plane component of the tip magnetization, which is due to the coating on the outer tip sides we used for test purposes.

The stability of the instrument and the use of nonmagnetic materials allows ramping the magnetic field and imaging simultaneously for more than 20 h at LHe temperature without readjustment of the tip-sample or fiber-cantilever distance. Thus it is possible to record the domain evolution in a movielike manner. This has been done with a 100-nm-thick $La_{0.7}Ca_{0.3}MnO_3$ film epitaxially grown on a $LaAlO_3$ (001) substrate. Such films exhibit a stress induced perpendicular anisotropy.[51] The Curie temperature of the imaged

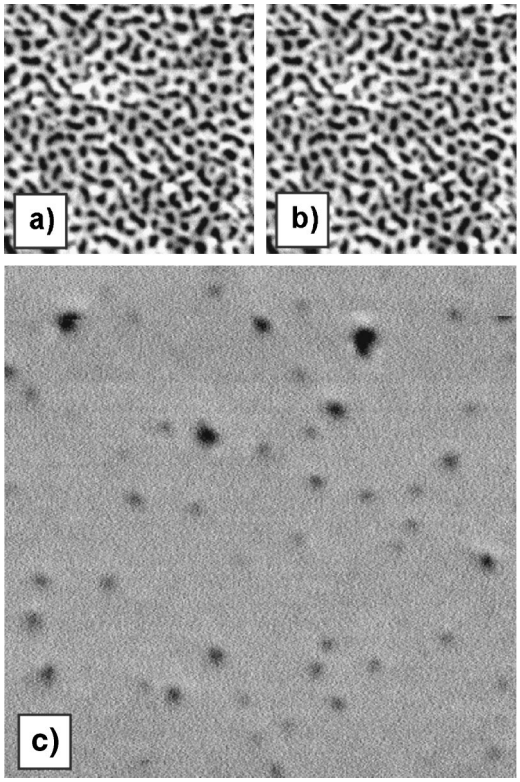

FIG. 7. MFM images of the domain structure of a 100-nm-thick $La_{0.7}Ca_{0.3}MnO_3$ film grown on a $LaAlO_3$ (001) substrate, recorded at 5.2 K with a 5 nm iron coating on the tip: (a) at 160 mT and (b) at 155 mT, (c) image difference of (a) and (b) elucidating the change of the domain structure within 5 mT. Parameters: scan area 4×4 μm^2, $f_0=193$ kHz, $A=\pm5$ nm, $h=30$ nm, $U_{bias}=1.5$ V, gray scale 370 mHz, scan speed 8 μm/s, bandwidth 100 Hz, $\delta f_{noise}=23$ mHz_{rms}.

film was 250 K, and the tip was coated with 5 nm iron on the side face towards the cantilever.

Figures 7(a) and 7(b) show two images of such a movie going from 0 T to saturation at 800 mT and back to 0 T within 22 h of measurement time. Each image has a field variation of 5 mT which is small enough to track changes of the domain configuration through several images. Due to the stability of the microscope and the use of nonmagnetic material, two consecutive images can be subtracted to directly visualize the changes of the domain structure. Figure 7(c) shows such a difference image. In spite of the fact that the domain pattern is maze type, the field dependent changes are still of cylindrical shape. Moreover, remaining topographic features can be eliminated by this method since they do not change with magnetic field.

ACKNOWLEDGMENTS

The authors would like to thank U. H. Pi and Z. G. Khim for providing the LCMO sample. Financial support from the DFG (Grant No. Wi 1277/13-1 and Graduiertenkolleg ''Physik nanostrukturierter Festkörper'') is gratefully acknowledged.

[1] G. Binnig, C. F. Quate, and C. Gerber, Phys. Rev. Lett. **56**, 930 (1986).
[2] C. B. Prater, M. R. Wilson, J. Garnaes, J. Massie, V. B. Elings, and P. K. Hansma, J. Vac. Sci. Technol. B **9**, 989 (1991).

[3] K. Nakamoto, C. B. Mooney, and M. Iwatsuki, Rev. Sci. Instrum. **72**, 1445 (2001).
[4] Q. Dai, R. Vollmer, R. W. Carpick, D. F. Ogletree, and M. Salmeron, Rev. Sci. Instrum. **66**, 5266 (1995).
[5] K. Suzuki, M. Iwatsuki, S. Kitamura, and C. B. Mooney, Jpn. J. Appl. Phys., Part 1 **39**, 3750 (2000).
[6] M. D. Kirk, T. R. Albrecht, and C. F. Quate, Rev. Sci. Instrum. **59**, 833 (1988).
[7] F. J. Giessibl, C. Gerber, and G. Binnig, J. Vac. Sci. Technol. B **9**, 984 (1991).
[8] T. R. Albrecht, P. Grütter, D. Rugar, and D. P. E. Smith, Ultramicroscopy **42-44**, 1638 (1992).
[9] H. J. Hug, A. Moser, T. Jung, O. Fritz, A. Wadas, I. Parashikov, and H.-J. Güntherodt, Rev. Sci. Instrum. **64**, 2920 (1993).
[10] C. W. Yuan, E. Batalla, M. Zacher, A. L. de Lozanne, M. D. Kirk, and M. Tortonese, Appl. Phys. Lett. **65**, 1308 (1994).
[11] R. Euler, U. Memmert, and U. Hartmann, Rev. Sci. Instrum. **68**, 1776 (1997).
[12] W. Allers, A. Schwarz, U. D. Schwarz, and R. Wiesendanger, Rev. Sci. Instrum. **69**, 221 (1998).
[13] D. V. Pelekhov, J. B. Becker, and G. Nunes, Jr., Rev. Sci. Instrum. **70**, 114 (1999).
[14] R. E. Thomson, Rev. Sci. Instrum. **70**, 3369 (1999).
[15] J. Rychen, T. Ihn, P. Studerus, A. Herrmann, and K. Ensslin, Rev. Sci. Instrum. **70**, 2765 (1999).
[16] H. J. Hug, B. Stiefel, P. J. A. van Schendel, A. Moser, S. Martin, and H.-J. Güntherodt, Rev. Sci. Instrum. **70**, 3625 (1999).
[17] P. Weitz, E. Ahlswede, J. Weis, K. v. Klitzing, and K. Eberl, Appl. Surf. Sci. **157**, 349 (2000).
[18] A. Volodin, K. Temst, C. van Haesendonck, and Y. Bruynseraede, Rev. Sci. Instrum. **71**, 4468 (2000).
[19] M. Roseman and P. Grütter, Rev. Sci. Instrum. **71**, 3782 (2000).
[20] N. Suehira, Y. Tomiyoshi, Y. Sugawara, and S. Morita, Rev. Sci. Instrum. **72**, 2971 (2001).
[21] A. Schwarz, W. Allers, U. D. Schwarz, and R. Wiesendanger, Appl. Surf. Sci. **140**, 293 (1999).
[22] W. Allers, A. Schwarz, U. D. Schwarz, and R. Wiesendanger, Appl. Surf. Sci. **140**, 247 (1999).
[23] W. Allers, A. Schwarz, U. D. Schwarz, and R. Wiesendanger, Europhys. Lett. **48**, 276 (1999).
[24] W. Allers, S. M. Langkat, and R. Wiesendanger, Appl. Phys. A: Mater. Sci. Process. **72**, S27 (2001).
[25] M. A. Lantz, H. J. Hug, P. J. A. van Schendel, R. Hoffmann, S. Martin, A. Baratoff, A. Abdurixit, H.-J. Güntherodt, and C. Gerber, Phys. Rev. Lett. **84**, 2642 (2000).
[26] N. Suehira, Y. Sugawara, and S. Morita, Jpn. J. Appl. Phys., Part 2 **40**, L292 (2001).
[27] Omicron Vacuumphysics, Taunusstein, Germany.
[28] Pfeiffer Vacuum Technologies AG, Asslar, Germany.
[29] Varian Vacuum Technologies, Lexington, MA.
[30] Vacuum Generators, Hastings, UK.
[31] CryoVac, Troisdorf, Germany.
[32] American Magnetics, Inc., Oak Ridge, TN.
[33] G. K. White, *Experimental Techniques in Low-Temperature Physics* (Oxford University Press, Oxford, 1979).
[34] R. Berman, J. Appl. Phys. **27**, 318 (1956).
[35] R. Berman and C. F. Mate, Nature (London) **182**, 1661 (1958).
[36] J. G. Hust, Rev. Sci. Instrum. **41**, 622 (1970).
[37] Torr Seal, Varian Vacuum Technologies, Lexington, MA.
[38] MACOR is a trademark of Corning Glass Works and denotes a machinable glass ceramic.
[39] G. Nunes, Jr. and D. Williams, J. Vac. Sci. Technol. B **13**, 1063 (1995).
[40] D. Rugar, H. J. Mamin, and P. Güthner, Appl. Phys. Lett. **55**, 2588 (1989).
[41] Sony Laser Diode SLD 201 V-3, $\lambda = 781$ nm.
[42] We use cantilever holders with a tilting angle of 15° produced by Omicron Vacuumphysics, Taunusstein, Germany.
[43] Staveley Sensors Inc., East Hartford, CT. EBL 4 denotes industry type PZT-8.
[44] EBL data sheet, Staveley Sensors Inc., East Hartford, CT.
[45] M. E. Taylor, Rev. Sci. Instrum. **64**, 154 (1993).
[46] S. H. Pan, S. Behler, M. Bernasconi, and H.-J. Güntherodt, Bull. Am. Phys. Soc. **37**, 167 (1992).
[47] Chr. Wittneven, R. Dombrowski, S. H. Pan, and R. Wiesendanger, Rev. Sci. Instrum. **68**, 3806 (1997).
[48] We used a silicon grid with 2 μm periodicity, manufactured by TM Microscopes, formerly TopoMetrix Corporation, Sunnyvale, CA.
[49] Lake Shore Cryotronics, Inc., Westerville, OH.
[50] T. R. Albrecht, P. Grütter, D. Horne, and D. Rugar, J. Appl. Phys. **69**, 668 (1991).
[51] M. C. Smoak, P. A. Ryan, and F. Tsui, J. Appl. Phys. **87**, 6764 (2000).